Improved LTE like initial uplink synchronization via reduced problem dimension

Md Mashud Hyder, Kaushik Mahata

PII: S0140-3664(19)30068-4
DOI: https://doi.org/10.1016/j.comcom.2019.05.015
Reference: COMCOM 5870

To appear in: *Computer Communications*

Received date : 18 January 2019
Revised date : 14 April 2019
Accepted date : 17 May 2019

Please cite this article as: M.M. Hyder and K. Mahata, Improved LTE like initial uplink synchronization via reduced problem dimension, *Computer Communications* (2019), https://doi.org/10.1016/j.comcom.2019.05.015

Improved LTE like initial uplink synchronization via reduced problem dimension

Md Mashud Hyder and Kaushik Mahata

Abstract

Initial uplink synchronization (IUS) is a random access process in LTE that enables the eNodeB to detect, and uplink synchronize new user equipment. In future networks with huge number of devices, the number of simultaneous IUS users will increase significantly. In addition, it is desirable to serve users moving at high speed. We exploit the structure of the physical random access channel (PRACH) in LTE to reduce the dimension of the underlying data model. This reduction gives a very compact representation of channel impulse response (CIR). We utilize this representation to develop an efficient algorithm which can work in presence of large multiple access interference (MAI) and high carrier frequency offsets (CFO). When compared with the state of the art methods. the proposed method is capable of detecting a significantly higher number of IUS users and can allow high values of CFO. In addition, it produces very reliable estimates of both CIR and CFO of the detected users.

Keywords: Random Access, initial uplink synchronization, subspace dimension reduction.

I. Introduction

A. Background

LTE uses single carrier frequency-division multiple access (SC-FDMA) in uplink. This requires the uplink signals from different user equipments (UEs) to be aligned in time, and have nearly the same power level when they arrive at the eNodeB. This is possible only if each UE delays and amplifies its uplink transmission appropriately to compensate for the delay and the gain associated with its channel impulse response (CIR). For a new UE the delay and gain parameters are unknown. Hence LTE requires every new UE to undergo a network entry procedure called the Initial Uplink Synchronization (IUS). Each UE

Research is supported by the Australian Research Council.

Department of Electrical Engineering, The University of Newcastle, NSW 2308, Australia. E-mail: md.hyder@uon.edu.au; Kaushik.Mahata@newcastle.edu.au

wanting to enter the network uses some downlink control signals to downlink synchronizes itself with eNodeB by estimating the relevant frequency. An UE uses its estimates of downlink channel parameters during IUS. IUS is a contension based random access (RA) process. The LTE standard specifies certain special time slots when UEs are given the so-called "RA opportunity". Furthermore, LTE allocates a set of carrier frequencies called physical random access channel (PRACH) for RA data transmission. A downlink synchronized UE wanting to enter the network, also refered to as a Random Access Terminal (RT), must select an RA opportnity to transmit a code over the PRACH. The code must be chosen at random from a pre-specified codebook. Note that at a particulat RA opportunity, multiple RTs can transmit signals. The signals transmitted by all RTs participating in an RA opportunity are superimposed on each other in the channel, and the resulting signal is received by the eNodeB. The eNodeB uses this received signal to detect the transmitted codes, and for each detected code the eNodeB estimates the corresponding CIR, propagation delay and the carrier frequency offset (CFO) [1]–[3]. The detected codes and the corresponding CIR power, propagation delay and CFO estimates are subsequently broadcast by the eNodeB in a response message. Now the UEs can use this information to properly delay their uplink transmission and select appropriate transmit power levels. Note that if multiple RTs transmit same code then collision occurred in the transmission and the IUS process of associated RTs become unsuccessful. Similar random access processes has also been adopted in WiMAX (IEEE 802.16 wireless metropolitan area network).

Multiuser code detection and their corresponding CIR, propagation delay and CFO estimation are the main task of IUS. Among the state of the art methods, [4] utilizes a set of generalized chirp-like polyphase sequences to get sharp time delay estimates. The work in [5] demonstrates that the frequency-domain correlation approach outperforms its time domain counterpart for IUS parameter estimation. The method proposed in [6] allocates a small number of subcarriers to each ranging opportunity so that most of the RTs are expected to transmit on disjoint sets of subcarriers with minimum level of MAI. However, the reduction of the number of effective subcarrier for each user results in the degradation of timing estimation performance [1]. A similar approach has been proposed in [7] for channel synchronization. This method assumes that the uplink signals are transmitted over disjoint subcarriers, and the receivers use filter banks to separate multiuser codes. An iterative parallel interference cancellation (IPIC)-based multiuser detection and estimation algorithm is proposed in [8] for the coordinated multipoint (CoMP) transmission in LTE system. The authors also proposed a RA subchannel allocation scheme which can suppress mutual interference between coordinated users and noncoordinated users. The work in [9] improves the IUS performance by dividing the ranging signals into several groups with each group being transmitted over exclusively assigned subcarriers. The iterative maximum likelihood algorithm in [10] applied an

expectation-maximization (EM) type technique to mitigate MAI in the user detection process. Successive interference cancellation (SIC) algorithms [1]–[3] are very popular in IUS for their low complexity and efficient user detection capability. In its most basic form, the algorithm works in an iterative fashion where the strongest path of each active RT is detected and is removed from the received signal and the resulting signal is used in succeeding iterations. In [11] a sparse recovery framework is proposed. The theory is used in [12] to optimally select the Zadoff-Chu (ZC) codes in the RA codebook, and in [13] for a fast SIC algorithm. The non-linear distortion of transmission signal over multipath fading channel in LTE system is analyzed in [14] which helps to understand the inter-distortion interference (IDI) between multiple users and improve IUS performance. Multi-user timining offset estimation in a random access environment for massive multiple-input multiple-output (MIMO) systems is proposed in [15]. The spatial degrees of freedom provided by massive MIMO systems are used together with the inherent different time instants of reception of UEs' signals to resolve inter-user collisions. Finally a subspace based algorithm is applied to estimate timing offset of different users.

In the LTE context, there are two main shortcomings of the approaches outlined above [1]–[3], [11], [12]. Firstly, when the channel power of the UEs vary over a wide range (due to different locations of users in a wireless cell), then the UEs with small channel power are very hard to detect. Secondly, the IUS algorithms [1]–[3], [6], [7], [16] assume CFO is negligible. Indeed, in 2.5 GHz LTE with format-0 PRACH [17], (see also Table-I), the CFO due to errors in the frequency synthesizer is typically less than 400 Hz, which is about 30% of the PRACH subcarrier spacing. However it is increasingly desirable to be able to synchorize UEs moving at high speed. Then, due to Doppler effect, the CFO would be significantly higher. The recent RA codebook design in [12] attempts to make the codebook robust to the adverse effects of CFO. However, the hybrid algorithm of [18] is the only method for joint CFO estimation and user detection. Unfortunately, its user detection performance is very sensitive to channel SNR variation (see [13, Figure 2]).

The future networks are expected to connect huge number of devices [19]. This will increase the number of simultaneous IUS requests by a considerable proportion. Now the RA process assumes that the number of codes G in the RA codebook is much larger than the number of simultaneous requests. The probability that a particular code is transmitted by an RT is $1/G$. If there are n RTs, then the probability that a code is transmitted by no more than one RT is $(1-G^{-1})^n + nG^{-1}(1-G^{-1})^{n-1}$. This probability of a collision-free IUS should be as close to 1 as possible. For LTE, $G = 64$. Hence with $n = 5$ the probability of collision free IUS is 0.85. To serve a larger number of RTs with the same probability of collision-free IUS we must increase G. For instance, to support $n = 10$ with the same confidence we need $G \geq 150$. However, an increase in G does not only increase the complexity of the IUS methods,

but also severely affect their detection-estimation accuracy. Therefore it is of considerable interest to seek alternative solutions capable of delivering acceptable detection-estimation performance for a significantly larger codebook size G at some moderate computational complexity. At the same time it is desirable to be able to serve UEs moving at a high speed, and cater for UEs with widely varying channel power.

B. Contributions

In this paper we aim to address the above challenges by exploiting certain mathematical property of LTE-PRACH and its impact on the signal model. We show that the underlying dimension of the IUS problem is significantly smaller than what was thought before. To understand this in a simple way, first consider the scenario where the RTs have negligible CFOs. Then the previous research has shown that the signal $\boldsymbol{y}$ received by the eNodeB in a particular RA opportunity can be expressed as, see *e.g.* [12],

$$\boldsymbol{y} = \sum_{\ell=1}^{G} \boldsymbol{\Gamma}_\ell \bar{\boldsymbol{h}}_\ell + \boldsymbol{e}, \tag{1}$$

where G is the number of codes in the codebook, and $\boldsymbol{e}$ is the additive measurement noise vector. The vector $\bar{\boldsymbol{h}}_\ell$ depends on the CIR of the RT transmitting the ℓ-th code in the codebook. It's length N_1 depends on the cell radius and the maximum CIR length in the system (see discussion around (8) for detail). Note that $\|\bar{\boldsymbol{h}}_\ell\|_2 = 0$ if the ℓ-th code does not transmitted by any RT. The signal $\boldsymbol{y}$ is of dimension M, where M is the number of adjacent subcarriers in the PRACH. The matrices $\{\boldsymbol{\Gamma}_\ell\}_{\ell=1}^{G}$ are known. In particular, we can calculate $\boldsymbol{\Gamma}_\ell$ if we know that the ℓ th code in the codebook. Therefore, the IUS problem involves solving the unknown vector

$$\hat{\boldsymbol{h}} = [\ \bar{\boldsymbol{h}}_1^\intercal \ \ \bar{\boldsymbol{h}}_2^\intercal \ \ \cdots \ \ \bar{\boldsymbol{h}}_G^\intercal\ ]^\intercal.$$

of dimension $N_1 G$ from M noisy linear measurements, where $(.)^\intercal$ denotes transpose. In a practical LTE system with a cell radius 2.1 km we have $N_1 = 530$. In addition, $M = 839$ and $G = 64$. This means we have $N_1 \times G = 33920$ unknowns in (1), which needs to be solved from 839 noisy measurements. This is an ill posed task in absence of any further information.

To handle the above problem, the state-of-the-art methods exploit the fact that in reality, the number n of active RTs is actually a lot smaller than G. Hence in reality, the majority of $\{\bar{\boldsymbol{h}}_\ell\}_{\ell=1}^{G}$ are zero vectors. The number of non-zero entries in $\hat{\boldsymbol{h}}$ is a bit less than nN_1. In the following the non-zero entries in $\hat{\boldsymbol{h}}$ will be denoted by K. However, we don't know those few values of ℓ for which $\bar{\boldsymbol{h}}_\ell \neq 0$. This makes the detection-estimation problem a sparse signal recovery problem. Indeed, some recent algorithms for solving the IUS problem use the principles of sparse recovery. The SIC algorithms in [1]–[3], [13] can be viewed as special variants of the class of matching persuit algorithms [20]. The algorithm in [11] uses a mix of ℓ_0 and ℓ_1 minimization strategy.

How well a sparse signal recovery problem can be solved, depends on three integers: *i)* The number of unknowns, which is N_1G in above; *ii)* The number of measurements, which is M in our case; and *iii)* The number K of non-zero components in the unknown vector $\hat{\boldsymbol{h}}$. In above K is proportional to the number n of active RTs. The theory of sparse signal recovery suggests that for a given M, and the number of unknowns, we will achieve better detection-estimation result if the value of K is reduced. This explains why the existing algorithms produce good results for smaller values of n. If n increases then K increases proportionally, and eventually $\hat{\boldsymbol{h}}$ is no longer sparse enough for the estimation methods to succeed. In such cases one may expect some improvement in the results if the number of unknowns is somehow reduced. In this paper we describe a way to accomplish exactly that. We propose a new parameterization such that we can work with a significantly smaller number of unknowns, and yet, the unknown vector retains the same level of sparsity, *i.e.* the ratio of the number of non-zero entries in the unknown vector to the dimension of the unknown vector remains almost the same.

Recall that N_1 is the number of columns in $\boldsymbol{\Gamma}_\ell$. Our work is founded on the observation that the dimension of the column space of $\boldsymbol{\Gamma}_\ell$ is much much smaller than N_1. This is true for any ℓ. In particular we show in Appendix that the dimension of the column space of $\boldsymbol{\Gamma}_\ell$ is $\lceil MN_1/N \rceil$, where N is the number of OFDM subcarriers used in the system. In an LTE system employing $M = 839$ one has $N = 24576$. For a cell of 2.1 km radius $N_1 = 530$. Hence the matrix $\boldsymbol{\Gamma}_\ell$ is of size 839×530. But its column space is of dimension $\lceil \frac{839\times 530}{24576} \rceil = 19$ only.

Consider an $M \times \lceil MN_1/N \rceil$ matrix $\mathbf{U}_\ell$ be such that its columns form an orthogonal basis of the column space of $\boldsymbol{\Gamma}_\ell$. We can calculate such an $\mathbf{U}_\ell$ in many ways like the QR factorization of $\boldsymbol{\Gamma}_\ell$. Since the columns of $\mathbf{U}_\ell$ are mutually orthogonal for any given $\bar{\boldsymbol{h}}_\ell$, there is a unique $\lceil MN_1/N \rceil$ dimensional vector $\boldsymbol{h}_\ell$ such that

$$\boldsymbol{\Gamma}_\ell \bar{\boldsymbol{h}}_\ell = \mathbf{U}_\ell \boldsymbol{h}_\ell.$$

In addition $\boldsymbol{h}_\ell = 0$ whenever $\bar{\boldsymbol{h}}_\ell = 0$. Since $\bar{\boldsymbol{h}}_\ell \neq 0$ for only a few values of ℓ corresponding to the codes transmitted by the active RTs, we conclude that $\bar{\boldsymbol{h}}_\ell \neq 0$ for those few values of ℓ corresponding to the transmitted codes. With these observations, we can now cast the detection-estimation problem under consideration in terms of $\{\boldsymbol{h}_\ell\}_{\ell=1}^{G}$ where (1) is rewritten as

$$\boldsymbol{y} = \sum_{\ell=1}^{G} \mathbf{U}_\ell \boldsymbol{h}_\ell + \boldsymbol{e}. \tag{2}$$

Now our objective is to find $\{\boldsymbol{h}_\ell\}_{\ell=1}^{G}$. We can also account for the sparsity, by devising an estimation strategy that attempts to maximize the number of zero vectors in the solution set $\{\boldsymbol{h}_\ell\}_{\ell=1}^{G}$. In the specific LTE scenario discussed before, $M = 839$ and total the number of unknowns is $19 \times G = 19 \times 64 = 1216$. According to the theory of sparse signal recovery, this problem is a lot easier than the original problem.

We shall demonstrate that the above modified formulation has several additional advantages. The dramatic reduction in the number of unknowns per code makes way for larger codebooks. For a fixed M we can now increase G and still the total number of unknowns can be kept within a manageable limit. That in turn allows more active RTs, and still avoid collisions during the random access process. In the above discussion we have assumed that the CFO of an active RT is negligible. However, we shall see later that the reduced number of unknowns in (2) allows us to account for the CFOs, and solve them along with $\{\boldsymbol{h}_\ell\}_{\ell=1}^G$ in a rather reliable manner. The reduced problem dimension brings computational advantages as well. We demonstrate these advantages by proposing a SIC type detection algorithm. The detection step yields estimates of $\{\boldsymbol{h}_\ell\}_{\ell=1}^G$. Subsequently, we use these to estimate the CIR and CFO. The underlying algorithm employs the maximum likelihood principle, and thus, is very accurate. The utility of the proposed approach is demonstrated via simulation study.

II. Signal model

In this section we briefly review the signal model for the IUS problem in an LTE like system. The description below closely follows the derivation in [12]. LTE system uses orthogonal frequency division multiple access (OFDMA). As mentioned before, we use N to denote the number of subcarriers. Each subcarrier carries one discrete-time data sample. Thus, an OFDM frame carries N discrete-time data samples. Out of the N subcarriers, a set of M adjacent subcarriers are allocated for the PRACH.

Recall that the RA codebook consists of G codes. We denote them by $\boldsymbol{c}_1, \boldsymbol{c}_2, \ldots, \boldsymbol{c}_G$. Each of these codes is an M dimensional vector, derived by computing an M point discrete Fourier transform of a Zodoff-Chu sequence, see [17] for details. See [12] for guidelines to choose better codes. During an RA opportunity an RT, say T, calculates these N samples by calculating the N point inverse discrete Fourier transform of the chosen code $\boldsymbol{c}_\ell$. In particular, the q th data sample $s(q)$ is given by

$$s(q) = \frac{1}{\sqrt{N}} \sum_{m=1}^{M} \boldsymbol{c}_\ell(m) \ \exp\{\mathrm{i}2\pi j_m q/N\}, \ q = \mathcal{I}, \tag{3}$$

where $\boldsymbol{c}_\ell(m)$ denotes the m th component of $\boldsymbol{c}_\ell$. In addition, j_m is the index of m-th PRACH subcarrier, and we denote $\mathcal{I} := \{0, 1, \ldots, N-1\}$. Apart from the data-samples an OFDM frame contains its usual cyclic prefix. In the sequel N_p denotes the length of the cyclic prefix. In addition, the frame transmitted during an RA opportunity contains N_g additional guard samples. Together the data samples, the cyclic prefix and the guard samples are concatenated to generate N_p+N+N_g channel symbols. We denote these channel symbols by $w(k), k = -N_p, \ldots, -1, 0, 1, \ldots, N+N_g-1$. In particular, these are constructed from $s(q), \ q \in \mathcal{I}$ as

$$w(k) = \begin{cases} s(k \bmod N), & -N_p \le k \le N-1, \\ 0, & N \le k \le N+N_g-1, \end{cases} \tag{4}$$

Note that $(k \bmod M) := k - M \cdot \lfloor \ell/M \rfloor$, with $\lfloor r \rfloor$ denoting the largest integer less than or equal to r.

Suppose $h(p),\ p \in \{0, 2, \cdots P-1\}$ are the uplink channel impulse response (CIR) coefficients between the transmitter T and eNodeB where P is the channel length. Discarding the cyclic prefix and the guard symbols, let $\{v(k)\}_{k=0}^{N-1}$ be the contribution of T in the symbols received by the eNodeB during the RA opportunity. These are delayed and convoluted version of the transmitted symbols. For $k \in \mathcal{I}$, the received signal at eNodeB be

$$\begin{aligned}\tilde{v}(k) &= \mathrm{e}^{\mathrm{i}2\pi k\epsilon_\ell/N} \sum_{p=d}^{d+P-1} h(p-d)\ w(k-p), \\ &= \mathrm{e}^{\mathrm{i}2\pi k\epsilon_\ell/N} \sum_{p=d}^{d+P-1} h(p-d)\ s\{(k-p) \bmod N\}, \end{aligned} \tag{5}$$

where the propagation delay d depends on the distance between T and eNodeB, and ϵ_ℓ is the CFO (normalized by subcarrier spacing).

The eNodeB computes the N point DFT of the $\boldsymbol{v}$ of the vector $\tilde{\boldsymbol{v}} := [\ \tilde{v}(0)\ \ \tilde{v}(1) \cdots\ \ \tilde{v}(N-1)\ ]^\intercal$, where $(.)^\intercal$ denotes transpose. Then it can be shown that (see [12, eq. (15)])

$$\boldsymbol{v} = \mathbf{Q}_\ell \mathrm{diag}(\boldsymbol{c}_\ell)\boldsymbol{\Theta}\mathbf{F} \begin{bmatrix} \mathbf{0}_{1\times 1} \\ h_0 \\ h_1 \\ \vdots \\ h_{P-1} \\ \mathbf{0}_{(N-P-d)\times 1} \end{bmatrix} \tag{6}$$

$$\mathbf{Q}_\ell = \mathbf{I}_M + \mathbf{H}\epsilon_\ell + O(\epsilon_\ell^2),$$

$$\text{where} \quad \mathbf{H}_{(k,l)} = \begin{cases} \mathrm{i}\pi(1-1/N), & k = l, \\ -\frac{\pi \mathrm{e}^{\mathrm{i}\pi(k-l)/N}}{N\sin(\pi(k-l)/N)}, & k \neq l. \end{cases} \tag{7}$$

Here $\mathbf{F}$ is the $N \times N$ DFT matrix:

$$[\mathbf{F}]_{k,m} = \exp\{-\mathrm{i}2\pi(k-1)(m-1)/N\}/\sqrt{N},$$

$\boldsymbol{\Theta}$ is an $M \times N$ row selector matrix such that m-th row of $\boldsymbol{\Theta}$ is the j_m-th row of the $N \times N$ identity matrix, $\mathbf{I}_M$ is $M \times M$ identity matrix, $\mathbf{0}_{1\times d}$ is a d-vector with all zeros.

Let $P_{\max}$ be the maximum value of P, and D be the maximum value of d. Denote $N_1 = P_{\max} + D$. Then, $d + P - 1 \le N_1$. Thus, all rows of

$$[\ \mathbf{0}_{1\times d}\ \ h_0\ \ h_1\ \ \cdots\ \ h_{P-1}\ \ \mathbf{0}_{1\times(N-P-d)}\ ]^\intercal \tag{8}$$

with indices larger than N_1 are zeros. Hence we can write (6) as

$$\boldsymbol{v} = \mathbf{Q}_\ell \text{diag}(\boldsymbol{c}_\ell)\boldsymbol{\Theta}\mathbf{F}_{(:,1:N_1)}\mathfrak{s}(\boldsymbol{h}, d), \tag{9}$$

where we use the Matlab notation $\mathbf{F}_{(:,1:N_1)}$ to denote the sub-matrix of $\mathbf{F}$ consisting of its first N_1 columns, we define the N_1 dimensional vector valued function

$$\mathfrak{s}(\boldsymbol{h}, d) = [\ \mathbf{0}_{1\times d}\ \ \boldsymbol{h}^\intercal\ \ \mathbf{0}_{1\times(N_1-P-d)}\ ]^\intercal \tag{10}$$

of a $P \leq P_{\max}$ dimensional vector $\boldsymbol{h} = [\ h_0\ \ h_1\ \ \cdots\ \ h_{P-1}\ ]^\intercal$ and an integer $d \leq D_{\max}$. In a practical system both $P_{\max}$ and D are known. Therefore, we can estimate N_1 [1], [2].

III. A COMPACT BLOCK SPARSE SIGNAL MODEL

In the Appendix we show that $\boldsymbol{\Theta}\mathbf{F}_{(:,1:N_1)}$ has only $\tau = \lceil MN_1/N \rceil$ significant singular values, and the remaining singular values are very close to zero. This result holds when $N \gg M$, which is true for the practical LTE systems. Hence we can very accurately approximate $\boldsymbol{\Theta}\mathbf{F}_{(:,1:N_1)} = \mathbf{U}\boldsymbol{\Sigma}\mathbf{V}^*$. $\mathbf{U}$ is an $M \times \tau$ matrix with its columns being the τ mutually orthogonal left singular vectors of $\boldsymbol{\Theta}\mathbf{F}_{(:,1:N_1)}$ corresponding to its τ significant singular values. Similarly $\mathbf{V}$ is an $N_1 \times \tau$ matrix with the τ significant right singular vectors of $\boldsymbol{\Theta}\mathbf{F}_{(:,1:N_1)}$ as its columns and $\mathbf{V}^*$ denotes complex conjugate transpose. $\boldsymbol{\Sigma}$ is the $\tau \times \tau$ diagonal matrix of the significant singular values.

Now consider a IUS opportunity where several RTs transmit simultaneously. Let $\boldsymbol{h}_\ell$ be the CIR vector of the RT sending code $\hat{\boldsymbol{c}}_\ell$, and d_ℓ be its propagation delay. Then the received data $\boldsymbol{y}$ at eNodeB is obtained by adding the contributions of the form (9) from all the RTs:

$$\boldsymbol{y} = \sum_{\ell=1}^{G} \mathbf{Q}_\ell \text{diag}(\boldsymbol{c}_\ell)\boldsymbol{\Theta}\mathbf{F}_{(:,1:N_1)}\mathfrak{s}(\boldsymbol{h}_\ell, d_\ell) + \boldsymbol{e}, \tag{11}$$

where $\boldsymbol{e}$ is the additive measurement noise. In practice, the number of active RTs is much smaller than G. If $\hat{\boldsymbol{c}}_\ell$ is not sent for a particular ℓ then $\mathfrak{s}(\boldsymbol{h}_\ell, d_\ell) = 0$. Define

$$\boldsymbol{\xi}_\ell := \boldsymbol{\Sigma}\mathbf{V}^*\mathfrak{s}(\boldsymbol{h}_\ell, d_\ell), \tag{12}$$

$$\mathbf{A}_\ell := \text{diag}(\boldsymbol{c}_\ell)\mathbf{U}, \qquad \mathbf{B}_\ell := \mathbf{H}\mathbf{A}_\ell. \tag{13}$$

$$\mathbf{A} := [\ \mathbf{A}_1\ \mathbf{A}_2 \cdots \mathbf{A}_G\ ], \qquad \mathbf{B} := [\ \mathbf{B}_1\ \mathbf{B}_2 \cdots \mathbf{B}_G\ ] \tag{14}$$

Now substitute $\boldsymbol{\Theta}\mathbf{F}_{(:,1:N_1)} = \mathbf{U}\boldsymbol{\Sigma}\mathbf{V}^*$ in (11) and using the expression of $\mathbf{Q}_\ell$ from (7), we get

$$\boldsymbol{y} = \sum_{\ell=1}^{G} \mathbf{A}_\ell\boldsymbol{\xi}_\ell + \sum_{\ell=1}^{G} \epsilon_\ell\mathbf{B}_\ell\boldsymbol{\xi}_\ell + \boldsymbol{e}. \tag{15}$$

Now given $\boldsymbol{y}$, the IUS problem requires to estimate:

1) The indices of all active code, i.e., $\{\ell \in \{1, 2, \cdots G\} : \|\boldsymbol{\xi}_\ell\|_2 \neq 0\}$.
2) For each active code index ℓ, estimate the associated channel power $\|\boldsymbol{\xi}_\ell\|_2$, transmission delay d_ℓ and CFO ϵ_ℓ.

In LTE system, each $\boldsymbol{c}_\ell$ is obtained by computing the FFT of some Zodoff-Chu codes [17]. As a consequence, it turns out that each element of the vector $\boldsymbol{c}_\ell$ is of unit modulus [12]. As a result, the matrix $\mathrm{diag}(\boldsymbol{c}_\ell)$ becomes orthogonal. Therefore

$$\mathbf{A}_\ell^* \mathbf{A}_\ell = \mathbf{U}^* \mathrm{diag}(\boldsymbol{c}_\ell)^* \mathrm{diag}(\boldsymbol{c}_\ell) \mathbf{U} = \mathbf{I}_\tau \tag{16}$$

for all ℓ.

We note in passing an interesting implication of the model (15) when the LTE cell radious is amall and CFO is negligible [12], [16], [17], i.e., $\epsilon_\ell \approx 0$ for all ℓ. Consequently (15) reduces to

$$\boldsymbol{y} = \sum_{\ell=1}^{G} \mathbf{A}_\ell \boldsymbol{\xi}_\ell + \boldsymbol{e}.$$

If the cell radius is also small, then often $[\ \mathbf{A}_1 \ \cdots \ \mathbf{A}_G\ ]$ has more rows than columns. In that case we estimate $[\ \boldsymbol{\xi}_1^\intercal \ \cdots \ \boldsymbol{\xi}_G^\intercal\ ]^\intercal$ using linear least squares as $[\ \mathbf{A}_1 \ \cdots \ \mathbf{A}_G\ ]^\dagger \boldsymbol{y}$, where $(.)^\dagger$ denotes the Moore-Penrose pseudo-inverse operator. This estimator can be shown to be the minimum mean square error (MMSE) estimator [21] provided that the elements of $\boldsymbol{e}$ are independent and identically distibuted. We can detect users by applying a simple hypothesis test on the components of $[\ \mathbf{A}_1 \ \cdots \ \mathbf{A}_G\ ]^\dagger \boldsymbol{y}$ [21].

IV. SIC TYPE CODE DETECTION METHOD

If the cell radius is not small, then $[\ \mathbf{A}_1 \ \cdots \ \mathbf{A}_G\ ]$ has more columns than rows. In that case the above mentioned linear least squares approach is not applicable. Besides, it is desirable to be able to accommodate non-trivial CFO values in the system. In that case we must work with the complete model (15), and we are no longer able to apply the linear least squares method. For this reason we propose a code detection method for the model (15). It is an enhanced SIC [22] method. Let the set of all active RA code indices be

$$\mathcal{S} = \{\ell \in \{1, 2, \cdots G\} : \|\boldsymbol{\xi}_\ell\|_2 \neq 0\}, \tag{17}$$

Given the data $\boldsymbol{y}$ and an index $\ell \in \{1, 2, \ldots, G\}$, consider two hypotheses:

$$\mathcal{H}_0 : \ell \notin \mathcal{S}; \qquad \mathcal{H}_1 : \ell \in \mathcal{S}. \tag{18}$$

To decide in favor of one, we perform a generalized likelihood ratio test (GLRT) [23], [24]. To compute the associated test statistic we need the probability density function of $\boldsymbol{y}$ under each hypothesis. This is used to compute the maximum-likelihood (ML) estimates of unknown parameters in the probability

density function. Finally, the GLRT statistic is formed by plugging in the estimated values of the model parameters in the expressions of the probability density functions. In practice, the probability density functions are not given, but we need to device some realistic probability models. These models must be realistic in two ways. Firstly, ML estimation of the underlying model parameters must be a well posed problem. Secondly, we should be able to validate the model for the applications under consideration.

Under $\mathcal{H}_0$ we model $\boldsymbol{y}$ as a zero mean complex Gaussian random vector with a covariance matrix $\sigma_0^2\mathbf{I}_M$. The ML estimate of σ_0^2 is [25]

$$\hat{\sigma}_0^2 = \boldsymbol{y}^*\boldsymbol{y}/M. \tag{19}$$

Under hypothesis $\mathcal{H}_1$, we assume that $\boldsymbol{y}$ to be complex Gaussian with mean $\mathbf{A}_\ell\boldsymbol{\xi}_\ell$ and covariance matrix $\sigma_1^2\mathbf{I}_M$. By (16) $\mathbf{A}_\ell^*\mathbf{A}_\ell = \mathbf{I}_\tau$, and then the ML estimates of $\boldsymbol{\xi}_\ell$ and σ_1^2 are given by [25]

$$\hat{\boldsymbol{\xi}}_\ell = \mathbf{A}_\ell^*\boldsymbol{y}, \quad \hat{\sigma}_1^2 = \boldsymbol{y}^*(\mathbf{I}_M - \mathbf{A}_\ell\mathbf{A}_\ell^*)\boldsymbol{y}/M. \tag{20}$$

The Gaussian density function with mean $\boldsymbol{\mu}$ and covariance matrix $\sigma^2\mathbf{I}_M$ evaluated at $\boldsymbol{y}$ is given by

$$\mathcal{N}(\boldsymbol{y}, \boldsymbol{\mu}, \sigma^2) = (2\pi\sigma^2)^{-M/2}\exp\{-||\boldsymbol{y}-\boldsymbol{\mu}||_2^2/(2\sigma^2)\}.$$

Using (19) and (20) in above the GLRT statistic for our hypothesis testing problem is given by

$$\mathcal{L}(\boldsymbol{y}) := \frac{\mathcal{N}(\boldsymbol{y}, 0, \hat{\sigma}_0^2)}{\mathcal{N}(\boldsymbol{y}, \hat{\boldsymbol{\xi}}_\ell, \hat{\sigma}_1^2)} = \left(1 - \frac{\boldsymbol{y}^*\mathbf{A}_\ell\mathbf{A}_\ell^*\boldsymbol{y}}{\boldsymbol{y}^*\boldsymbol{y}}\right)^{M/2}. \tag{21}$$

Instead of working directly with the GLRT statistic (21) it is more convenient to work with a monotonic function thereof:

$$\mathcal{L}_1(\boldsymbol{y}) = \frac{1}{1 - \{\mathcal{L}(\boldsymbol{y})\}^{2/M}} - 1 = \frac{\boldsymbol{y}^*\breve{\mathbf{A}}_\ell\breve{\mathbf{A}}_\ell^*\boldsymbol{y}}{\boldsymbol{y}^*\mathbf{A}_\ell\mathbf{A}_\ell^*\boldsymbol{y}} \tag{22}$$

where $\breve{\mathbf{A}}_\ell$ is a $M \times (M-\tau)$ matrix with mutually orthogonal columns such that $\breve{\mathbf{A}}_\ell^*\mathbf{A}_\ell = 0$. While deriving (22) we use $\mathbf{A}_\ell\mathbf{A}_\ell^* + \breve{\mathbf{A}}_\ell\breve{\mathbf{A}}_\ell^* = \mathbf{I}_M$. This also implies that under $\mathcal{H}_0$ the covariance matrix of the complex Gaussian vector $\boldsymbol{y}^*[\mathbf{A}_\ell \;\; \breve{\mathbf{A}}_\ell]$ is $\sigma_0^2 I_M$; and hence $\mathcal{L}_1(\boldsymbol{y})$ is central F distributed with $2(M-\tau)$ and 2τ degrees of freedom. Hence we can apply an F-test on $\mathcal{L}_1(\boldsymbol{y})$. Denote by $F(\cdot)$ the central F distribution function with $2(M-\tau)$ and 2τ degrees of freedom. For a target false alarm probability q_{fa}, we decide $\mathcal{H}_0$ if $\mathcal{L}_1(\boldsymbol{y}) > \kappa = F^{-1}(1-q_{\text{fa}})$. Otherwise we decide $\mathcal{H}_1$.

We embed the above hypothesis testing approach in an SIC framework, where we successively remove the contributions of the detected codes from observed data to overcome the interference of the stronger sources on the others. We call it block successive interference cancellation (Blk-SIC) algorithm. The idea is outlined below:

1) Set $p = 1$ and $\boldsymbol{r}_1 = \boldsymbol{y}$. Construct an empty set $\mathbb{T} = \emptyset$, an empty matrix Ψ_0. Set $\kappa = F^{-1}(1-q_{\text{fa}})$.

2) Block index detection:

$$\mathbb{I} = \{\ell \in \{1, 2, \cdots G\} \backslash \mathbb{T} : \ \mathcal{L}_1(\boldsymbol{r}_p) \leq \kappa\}$$

3) If $\mathbb{I} = \emptyset$ then exit.

4) Set $\mathbb{T} = \mathbb{T} \ \cup \mathbb{I}$.

5) Update $\Psi_p = \left[\Psi_{p-1} \ \mathbf{A}_{\mathbb{I}(1)} \cdots \mathbf{A}_{\mathbb{I}(L)} \ \mathbf{B}_{\mathbb{I}(1)} \cdots \mathbf{B}_{\mathbb{I}(L)}\right]$, where L is the cardinality of the set $\mathbb{I}$.

6) Project $\boldsymbol{y}$ onto the null space of Ψ_p^*

$$\boldsymbol{r}_{p+1} = \mathbf{C}_p \boldsymbol{y} \tag{23}$$

where $\mathbf{C}_p = \mathbf{I}_M - \Psi_p(\Psi_p^* \Psi_p)^{-1} \Psi_p^*$.

7) $p = p + 1$

8) Goto Step 2.

9) Output: set of detected codes $\mathbb{T}$.

Blk-SIC initializes the set of all detected codes $\mathbb{T} = \emptyset$ and the residual as $\boldsymbol{r}_1 = \boldsymbol{y}$. At p-th iteration, Blk-SIC treats the residual $\boldsymbol{r}_p$ as the measured data and computes $\mathcal{L}_1(\boldsymbol{r}_p)$ for every block $\mathbf{A}_\ell, \ell \in \{1, 2, \cdots G\} \backslash \mathbb{T}$. It then selects the block indices $\mathbb{I}$ based on a threshold value κ. Once the block indices are chosen, the corresponding block matrices are concatenated with the matrix Ψ_p. Step-6 updates the residual $\boldsymbol{r}_{p+1}$ by projecting $\boldsymbol{y}$ onto the null space of Ψ_p^*.

We neglect the effect of $\mathbf{B}_\ell$ while calculating GLRT statistics in Step-2. However, while constructing Ψ_p in Step-6, we incorporate $\mathbf{B}_\ell$ also. To explain the reason recall (15). The vector $\boldsymbol{y}$ is constructed by $\mathbf{A}_\ell$ multiplied with $\boldsymbol{\xi}_\ell$ and $\mathbf{B}_\ell$ multiplied with $\epsilon_\ell \boldsymbol{\xi}_\ell$. Therefore, if ℓ is an active code index then we know that both $\|\boldsymbol{\xi}_\ell\|_2$ and $\|\epsilon_\ell \boldsymbol{\xi}_\ell\|_2$ are non-zero. Hence, we concatenate both $\mathbf{A}_\ell$ and $\mathbf{B}_\ell$ in Ψ_p. However, the energy of ϵ is generally very low ($\epsilon \leq 0.3$). Therefore, if we select codes based on GLRT statistics for $\mathbf{B}_\ell$ then the false alarm rate tends to increase.

A. Estimation of $\{\boldsymbol{\xi}_\ell, \epsilon_\ell\}_{\ell \in \mathcal{S}}$

Assuming $\mathcal{S}$ is known from the Blk-SIC algorithm described in the the previous section, we can rewrite (15) as

$$\boldsymbol{y} = \sum_{\ell \in \mathcal{S}} \mathbf{A}_\ell \boldsymbol{\xi}_\ell + \sum_{\ell \in \mathcal{S}} \mathbf{B}_\ell \epsilon_\ell \boldsymbol{\xi}_\ell + \boldsymbol{e} \tag{24}$$

where $\mathbf{A}_\ell, \mathbf{B}_\ell, \ell \in \mathcal{S}$ are known. Let the k th index in $\mathcal{S}$ be $\mathcal{S}(k)$. We propose to estimate $\{\boldsymbol{\xi}_\ell, \epsilon_\ell\}_{\ell \in \mathcal{S}}$ by solving the nonlinear least squares problem

$$\underset{\{\epsilon_\ell, \boldsymbol{\xi}_\ell\}_{\ell \in \mathcal{S}}}{\text{minimize}} \quad \left\| \boldsymbol{y} - \sum_{\ell \in \mathcal{S}} \mathbf{A}_\ell \boldsymbol{\xi}_\ell - \sum_{\ell \in \mathcal{S}} \epsilon_\ell \mathbf{B}_\ell \boldsymbol{\xi}_\ell \right\|^2 . \tag{25}$$

Note that (25) is motivated by the Gaussian maximum likelihood approach. However, this is a non-convex problem, and thus does not admit any known polynomial time algorithm for solution. Nevertheless, (25) is a bilinear least squares problem. We shall exploit this structure to device a two step algorithm. In Section IV-A1 we present a linear least squares and total least squares based non-iterative algorithm. In addition, we also have a more accurate, iterative alternating decent method. One may use the LS-TLS based estimates as initial estimates to kick start the alternating decent method.

1) Blk-SIC-TLS: We start by relaxing (25) where we work with a set of auxiliary unknowns

$$\boldsymbol{\zeta}_\ell = \boldsymbol{\xi}_\ell \epsilon_\ell, \quad \ell \in \mathcal{S}. \tag{26}$$

Subsequently, we obtain estimates of $\{\boldsymbol{\zeta}_\ell, \boldsymbol{\xi}_\ell\}_{\ell\in\mathcal{S}}$ by solving linear least squares problem

$$\underset{\{\boldsymbol{\zeta}_\ell, \boldsymbol{\beta}_\ell\}_{\ell\in\mathcal{S}}}{\text{minimize}} \quad \left\| \boldsymbol{y} - \sum_{\ell\in\mathcal{S}} \mathbf{A}_\ell \boldsymbol{\xi}_\ell - \sum_{\ell\in\mathcal{S}} \mathbf{B}_\ell \boldsymbol{\zeta}_\ell \right\|^2, \tag{27}$$

which is a relaxed version of (25). The analytical solution of the linear least squares problem is known, and we can readily compute the solution. We denote the associated estimates be $\{\hat{\boldsymbol{\xi}}_\ell, \hat{\boldsymbol{\zeta}}_\ell\}_{\ell\in\mathcal{S}}$.

Now we use the fact that ϵ_ℓ is real-valued, and in addition, $\boldsymbol{\zeta}_\ell = \boldsymbol{\xi}_\ell \epsilon_\ell$. Hence the real valued matrix

$$\begin{bmatrix} \mathrm{Re}(\boldsymbol{\xi}_\ell) & \mathrm{Re}(\boldsymbol{\zeta}_\ell) \\ \mathrm{Im}(\boldsymbol{\xi}_\ell) & \mathrm{Im}(\boldsymbol{\zeta}_\ell) \end{bmatrix} = \begin{bmatrix} \mathrm{Re}(\boldsymbol{\xi}_\ell) \\ \mathrm{Im}(\boldsymbol{\xi}_\ell) \end{bmatrix} \begin{bmatrix} 1 & \epsilon_\ell \end{bmatrix}$$

is a rank-1 matrix. Using this information we use a total least squares method to find improved estimates of $\{\boldsymbol{\xi}_\ell\}_{\ell\in\mathcal{S}}$. From these we shall derive estimates of $\{\epsilon_\ell\}_{\ell\in\mathcal{S}}$. For each $\ell \in \mathcal{S}$ we form the $2\tau \times 2$ real-valued matrices

$$\widehat{\mathbf{M}}_\ell = \begin{bmatrix} \mathrm{Re}(\hat{\boldsymbol{\xi}}_\ell) & \mathrm{Re}(\hat{\boldsymbol{\zeta}}_\ell) \\ \mathrm{Im}(\hat{\boldsymbol{\xi}}_\ell) & \mathrm{Im}(\hat{\boldsymbol{\zeta}}_\ell) \end{bmatrix}, \qquad \ell \in \mathcal{S}.$$

By the total least squares principle, the best rank-1 approximation of $\widehat{\mathbf{M}}_\ell$ is given by

$$\begin{bmatrix} \boldsymbol{u}_1 \\ \boldsymbol{u}_2 \end{bmatrix} \sigma \begin{bmatrix} w_1 \\ w_2 \end{bmatrix}^\intercal = \begin{bmatrix} \boldsymbol{u}_1 \\ \boldsymbol{u}_2 \end{bmatrix} \sigma w_1 \begin{bmatrix} 1 & \frac{w_2}{w_1} \end{bmatrix},$$

where σ is the largest singular value of $\widehat{\mathbf{M}}$, $[\ \boldsymbol{u}_1^\intercal \quad \boldsymbol{u}_1^\intercal\ ]^\intercal$ is the corresponding left singular vector, and $[\ w_1 \quad w_2\ ]^\intercal$ is the corresponding right singular vector. From here we get a refined estimates of $\boldsymbol{\xi}_\ell$ and ϵ_ℓ:

$$\check{\boldsymbol{\xi}}_\ell = (\boldsymbol{u}_1 + \mathrm{i}\boldsymbol{u}_2)\sigma w_1, \qquad \check{\epsilon}_\ell = \frac{w_2}{w_1}, \qquad \ell \in \mathcal{S}.$$

2) Blk-SIC-AD: Next we apply an alternating descent (AD) algorithm to solve (25). In this algorithm the Blk-SIC-TLS estimates could be used as initial guess. Recall that the number of active users is n. Hence the cardinality of $\mathcal{S}$ is n. We denote the ℓ th index in $\mathcal{S}$ by $\mathcal{S}(\ell)$. Let us define

$$\begin{aligned}
\boldsymbol{\epsilon} &= [\ \epsilon_{\mathcal{S}(1)} \quad \epsilon_{\mathcal{S}(2)} \quad \cdots \quad \epsilon_{\mathcal{S}(n)}\ ]^{\mathsf{T}}, \\
\overline{\boldsymbol{\xi}} &= [\ \boldsymbol{\xi}_{\mathcal{S}(1)}^{\mathsf{T}} \quad \boldsymbol{\xi}_{\mathcal{S}(2)}^{\mathsf{T}} \quad \cdots \quad \boldsymbol{\xi}_{\mathcal{S}(n)}^{\mathsf{T}}\ ]^{\mathsf{T}}, \\
\mathbf{W}(\boldsymbol{\epsilon}) &= [\ \mathbf{A}_{\mathcal{S}(1)} + \epsilon_{\mathcal{S}(1)}\mathbf{B}_{\mathcal{S}(1)} \quad \cdots \quad \mathbf{A}_{\mathcal{S}(n)} + \epsilon_{\mathcal{S}(n)}\mathbf{B}_{\mathcal{S}(n)}\ ], \\
\mathbf{Z}(\overline{\boldsymbol{\xi}}) &= [\ \mathbf{B}_{\mathcal{S}(1)}\boldsymbol{\xi}_{\mathcal{S}(1)} \quad \mathbf{B}_{\mathcal{S}(2)}\boldsymbol{\xi}_{\mathcal{S}(2)} \quad \cdots \quad \mathbf{B}_{\mathcal{S}(n)}\boldsymbol{\xi}_{\mathcal{S}(n)}\ ].
\end{aligned}$$

For a given $\boldsymbol{\epsilon}$ the cost function in (25) is minimized with respect to $\overline{\boldsymbol{\xi}}$ by taking $\overline{\boldsymbol{\xi}} = \mathbf{W}(\bar{\boldsymbol{\epsilon}})^{\dagger}\boldsymbol{y}$, where $\mathbf{W}(\bar{\boldsymbol{\epsilon}})^{\dagger}$ is the pseudo-inverse of $\mathbf{W}(\bar{\boldsymbol{\epsilon}})$. Similarly, for a given $\overline{\boldsymbol{\xi}}$ the cost function in (25) is minimized with respect to $\boldsymbol{\epsilon}$ by taking

$$\boldsymbol{\epsilon} = \begin{bmatrix} \mathrm{Re}\{\mathbf{Z}(\overline{\boldsymbol{\xi}})\} \\ \mathrm{Im}\{\mathbf{Z}(\overline{\boldsymbol{\xi}})\} \end{bmatrix}^{\dagger} \begin{bmatrix} \mathrm{Re}\left\{\boldsymbol{y} - \sum_{k=1}^{n} \mathbf{A}_{\mathcal{S}(k)}\boldsymbol{\xi}_{\mathcal{S}(k)}\right\} \\ \mathrm{Im}\left\{\boldsymbol{y} - \sum_{k=1}^{n} \mathbf{A}_{\mathcal{S}(k)}\boldsymbol{\xi}_{\mathcal{S}(k)}\right\} \end{bmatrix} \tag{28}$$

The alternating descent algorithm [26]–[28] solves (25) by iterating the above steps:

1) Set $\boldsymbol{\epsilon} = 0$ (or initialize $\boldsymbol{\epsilon}$ using the Blk-SIC-TLS estimates)
2) Compute $\overline{\boldsymbol{\xi}} = \mathbf{W}(\bar{\boldsymbol{\epsilon}})^{\dagger}\boldsymbol{y}$
3) Update $\boldsymbol{\epsilon}$ as in (28)
4) Exit if the change in the update $\boldsymbol{\epsilon}$ is below a predefined threshold; otherwise goto Step 2.

The alternating decent algorithm always converges monotonically to a stationary point of the cost function in (25) [27, Proposition-3]. We shall use $\{\mathring{\boldsymbol{\xi}}_\ell, \mathring{\epsilon}_\ell\}_{\ell\in\mathcal{S}}$ to denote the estimates obtained using the alternating decent algorithm.

B. Covariance matrix of $\{\mathring{\boldsymbol{\xi}}_\ell, \mathring{\epsilon}_\ell\}_{\ell\in\mathcal{S}}$

Let us denote

$$\begin{aligned}
\mathbf{G} &= [\mathbf{P}_1 \ \cdots \ \mathbf{P}_K \quad \widetilde{\mathbf{B}}_{\mathcal{S}(1)}\widetilde{\boldsymbol{\xi}}_{\mathcal{S}(1)} \ \cdots \ \widetilde{\mathbf{B}}_{\mathcal{S}(K)}\widetilde{\boldsymbol{\xi}}_{\mathcal{S}(K)}], \\
&\text{where, } \mathbf{P}_\ell = \widetilde{\mathbf{A}}_{\mathcal{S}(\ell)} + \widetilde{\mathbf{B}}_{\mathcal{S}(\ell)}\epsilon_{\mathcal{S}(\ell)}, \\
\widetilde{\mathbf{A}}_\ell &= \begin{bmatrix} \mathrm{Re}(\mathbf{A}_\ell) & -\mathrm{Im}(\mathbf{A}_\ell) \\ \mathrm{Im}(\mathbf{A}_\ell) & \mathrm{Re}(\mathbf{A}_\ell) \end{bmatrix}, \quad \widetilde{\mathbf{B}}_\ell = \begin{bmatrix} \mathrm{Re}(\mathbf{B}_\ell) & -\mathrm{Im}(\mathbf{B}_\ell) \\ \mathrm{Im}(\mathbf{B}_\ell) & \mathrm{Re}(\mathbf{B}_\ell) \end{bmatrix}, \\
\widetilde{\boldsymbol{\xi}}_\ell &= [\mathrm{Re}(\boldsymbol{\xi}_\ell)^{\mathsf{T}} \quad \mathrm{Im}(\boldsymbol{\xi}_\ell)^{\mathsf{T}}]^{\mathsf{T}}
\end{aligned}$$

If $\boldsymbol{e}$ is complex Gaussian with covariance matrix $\sigma^2\mathbf{I}$, then using the results available in [29] it can be verified that the large sample covariance matrix of $[\ \widetilde{\boldsymbol{\xi}}_{\mathcal{S}(1)}^{\mathsf{T}} \ \cdots \ \widetilde{\boldsymbol{\xi}}_{\mathcal{S}(n)}^{\mathsf{T}} \ \ \bar{\boldsymbol{\epsilon}}^{\mathsf{T}}]^{\mathsf{T}}$ is $\sigma^2(\mathbf{G}^{\mathsf{T}}\mathbf{G})^{-1}$. We need

to know the true values of $\{\boldsymbol{\xi}_\ell, \epsilon_\ell\}_{\ell\in\mathcal{S}}$ to compute this covariance matrix. In practice, the true values are unknown. Hence it is common to use the estimates $\{\mathring{\boldsymbol{\xi}}_\ell, \mathring{\epsilon}_\ell\}_{\ell\in\mathcal{S}}$ obtained from the alternating decent algorithm in lieu of the true values. The covariance computation requires σ^2 as well, and we can estimate that from the data. Let us define

$$\mathbf{D} = [\ \mathbf{A}_{\mathcal{S}_1} \ \cdots \ \mathbf{A}_{\mathcal{S}_n} \ \mathbf{B}_{\mathcal{S}_1} \ \cdots \ \mathbf{B}_{\mathcal{S}_n}\ ].$$

In (24) notice that $\boldsymbol{y} - \boldsymbol{e}$ resides in the column-space of $\mathbf{D}$. Hence it follows that

$$\boldsymbol{y}^*\{\mathbf{I}_M - \mathbf{D}(\mathbf{D}^*\mathbf{D})^{-1}\mathbf{D}^*\}\boldsymbol{y} = \boldsymbol{e}^*\{\mathbf{I}_M - \mathbf{D}(\mathbf{D}^*\mathbf{D})^{-1}\mathbf{D}^*\}\boldsymbol{e} = \mathrm{Tr}\{[\mathbf{I}_M - \mathbf{D}(\mathbf{D}^*\mathbf{D})^{-1}\mathbf{D}^*]\boldsymbol{e}\boldsymbol{e}^*\}.$$

Recall that $\boldsymbol{e}$ is zero mean complex random vector with covariance matrix $\sigma^2\mathbf{I}_M$. Hence

$$\mathsf{E}\{\boldsymbol{y}^*[\mathbf{I}_M - \mathbf{D}(\mathbf{D}^*\mathbf{D})^{-1}\mathbf{D}^*]\boldsymbol{y}\} = \sigma^2\mathrm{Tr}\{[\mathbf{I}_M - \mathbf{D}(\mathbf{D}^*\mathbf{D})^{-1}\mathbf{D}^*]\mathbf{I}_M\} = \sigma^2(M - 2n\tau).$$

Motivated by this result we estimate σ^2 by

$$\mathring{\sigma}^2 = \frac{\boldsymbol{y}^*\{\mathbf{I}_M - \mathbf{D}(\mathbf{D}^*\mathbf{D})^{-1}\mathbf{D}^*\}\boldsymbol{y}}{M - 2n\tau}.$$

This estimate can be used in place of σ^2 while calculating the joint covariance matrix of $\{\mathring{\boldsymbol{\xi}}_\ell, \mathring{\epsilon}_\ell\}_{\ell\in\mathcal{S}}$.

C. Timing offset estimation

In the final step of our algorithm we estimate timing offset for all $\ell \in \mathcal{S}$. Here we use the relations (12) and (10). In this section, we use the estimate $\{\mathring{\boldsymbol{\xi}}_\ell, \mathring{\epsilon}_\ell\}_{\ell\in\mathcal{S}}$ of $\{\boldsymbol{\xi}_\ell, \epsilon_\ell\}_{\ell\in\mathcal{S}}$ that was obtained by using the algorithms presented in the previous section.

1) Blk-SIC-CR: The first method is correlation (CR) based technique. Using $\mathring{\boldsymbol{\xi}}_\ell$ for some $\ell \in \mathcal{S}$ and applying the definition of $\boldsymbol{\xi}_\ell$ from (12), we compute an estimate of $\mathfrak{s}(\boldsymbol{h}_\ell, d_\ell)$ as $\boldsymbol{s}_\ell = \mathbf{V}\boldsymbol{\Sigma}\mathring{\boldsymbol{\xi}}_\ell$. Clearly $\boldsymbol{s}_\ell \in \mathbb{C}^{N_1}$. Then we estimate

$$d_\ell = \arg \max_{k\in\{1,2,\ldots,N_1\}} |\boldsymbol{s}_\ell(j)|.$$

This approach is motivated by (10) which shows that the index of the first nonzero component of $\mathfrak{s}(\boldsymbol{h}_\ell, d_\ell)$ is d_ℓ. In general, the components of the CIR vector $\boldsymbol{h}_\ell$ decays quickly. Therefore, we expect a few significant components of $\mathfrak{s}(\boldsymbol{h}_\ell, d_\ell)$ are centered around the index d_ℓ. This should result in high values in $|\boldsymbol{s}_\ell(j)|$ where j is close to d_ℓ.

2) Blk-SIC-ML: Using (10) note that the timing offset d_ℓ is the index of the first nonzero component of $\mathfrak{s}(\boldsymbol{h}_\ell, d_\ell)$. For any $\ell \in \mathcal{S}$, the alternating decent algorithm gives the maximum likelihood estimate of $\boldsymbol{\xi}_\ell = \boldsymbol{\Sigma}\mathbf{V}^*\mathfrak{s}(\boldsymbol{h}_\ell, d_\ell)$, see (12). In addition, we note that $\mathfrak{s}(\boldsymbol{h}_\ell, d_\ell)$ is a sparse vector (see (10)). We propose

TABLE I

SIMULATION PARAMETERS

Parameters	Notation	Values
Carrier Frequency	f_c	2.5 GHz
Sampling Frequency	f_n	30.72 MHz
Subcarrier Spacing	Δf	1.25 KHz
No. of RA Samples	N	24576
Cyclic Prefix (CP) Samples	N_p	3168
Total PRACH Subcarriers	M	839

to find a sparse vector valued estimate $\hat{\boldsymbol{\gamma}}_\ell$ of $\mathfrak{s}(\boldsymbol{h}_\ell, d_\ell)$ by solving the ℓ_1 norm minimization problem, see [11] and references therein,

$$\begin{aligned} \hat{\boldsymbol{\gamma}}_\ell = & \arg\min_{\boldsymbol{\gamma}} \|\boldsymbol{\gamma}\|_1 \\ & \text{subject to } \|\mathring{\boldsymbol{\xi}}_\ell - \boldsymbol{\Sigma}\mathbf{V}^*\boldsymbol{\gamma}\|_2 \leq \vartheta_\ell \end{aligned} \tag{29}$$

where ϑ_ℓ is a tuning parameter which controls the level of sparsity in $\hat{\boldsymbol{\gamma}}_\ell$. The index of the first nonzero component of $\hat{\boldsymbol{\gamma}}_\ell$ is taken as an estimate of d_ℓ. Note that we must solve (29) n times, once for each $\ell \in \mathcal{S}$, to estimate all $\{d_\ell\}_{\ell \in \mathcal{S}}$.

The value of ϑ should be proportional to the trace of the covariance matrix of $\mathring{\boldsymbol{\xi}}_\ell$. For this we need the covariance matrix expression given in Section IV-B.

V. SIMULATION RESULTS

The parameters of the simulated LTE system is provided in Table-I. As the RTs are located in different positions within the cell, their signals arrive at the eNodeB with different power levels. We simulate this by letting the signal to noise ratio (SNR) of each RT independent and uniformly distributed in $[0, Q]$ dB, where two different values of $Q = 20$ and 30 are considered. The SNR for ℓ-th RT is defined as SNR=$20\log_{10}(\|\boldsymbol{v}_\ell\|_2/\|\boldsymbol{e}\|_2)$ where $\boldsymbol{v}_\ell$ is the received signal at eNodeB from the RT (see (6)) and $\boldsymbol{e}$ is the noise contribution. At each simulation run the mobile speed s varies in the interval $[0, 25]$ m/s with uniform distribution. The wireless channels are modeled according to Extended Pedestrian A model (EPA) [30] if $s \leq 5$ m/s and Extended Vehicular A model (EVA) whenever $s > 5$ m/s. The maximum number of channel taps for any RT is 100. A cell radius of 2.1 km is assumed, which amounts to $N_1 = 530$. For the values of N_1, N and M we see that $\tau = 20$ is sufficient, i.e., 20 most significant eigenvalues of $\boldsymbol{\Theta}\mathbf{F}_{(:,1:N_1)}$ contains above 99.9% energy. The format of the PRACH is 0. As specified by the LTE

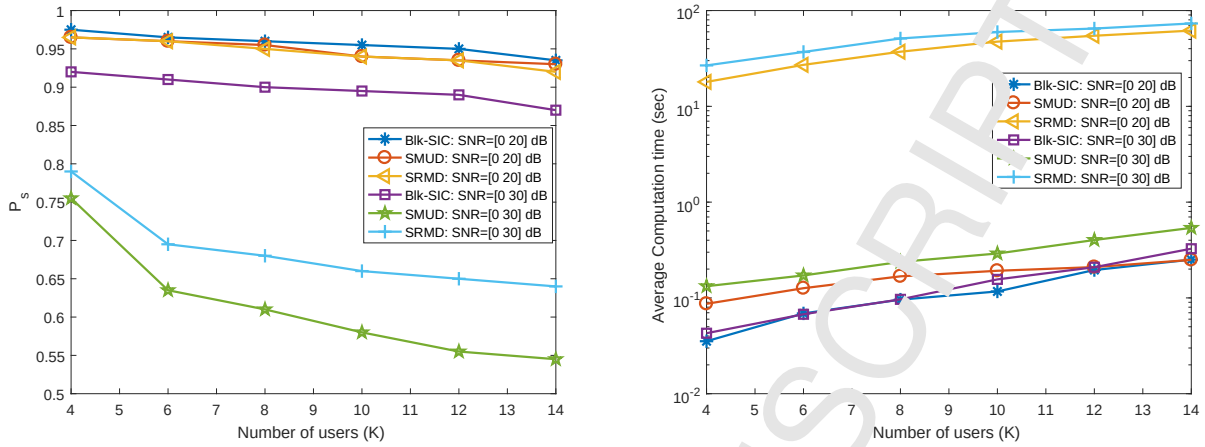

(a) (b)

Fig. 1. (a) Active code detection probability by different algorithms at low CFO. (b) Average computation time for different algorithms.

standard we derive the codes $\{\boldsymbol{c}_\ell\}_{\ell=1}^{G}$ are derived by computing the FFT of Zodoff-Chu (ZC) sequences. The u-th root ZC sequence Z^u is given element-wise as [31], [32]

$$Z^u(k) = \mathrm{e}^{-\mathrm{i}\pi u k(k+1)/M}, \quad k \in \{0, 1, \ldots, M-1\}. \tag{30}$$

where u is chosen from the Table 5.7.2-4 in [17]. The $(k+1)$-th element of $\boldsymbol{c}_{\ell+1}$ is given by

$$\boldsymbol{c}_{\ell+1,k+1} = \sum_{m=0}^{M-1} \mathrm{e}^{-\frac{\mathrm{i}2\pi k m}{M}} Z^u\left\{(m + \ell\, n_{cs}) \mod M\right\}. \tag{31}$$

We take a cyclic shift $n_{cs} = 26$ (see [17, Section-5]). To allow more RTs, we generate $G = 150$ codes. Note that for a given root u, we can generate maximum $\lfloor M/n_{cs} \rfloor = 26$ ZC preambles. Therefore we need 5 different roots to generate 150 codes. The roots are selected from [17, Table-5.7.2-4]) and codes are generated using (31). Recall that $\mathcal{S}$ denotes the set of all active RA code indices at a particular random access opportunity. Here $\hat{\mathcal{S}}$ denotes the set of all detected code indices. The probability that $\mathcal{S} = \hat{\mathcal{S}}$ is denoted by P_s. The false alarm probability $q_{\text{fa}} = 10^{-5}$ in Blk-SIC algorithm. Two successive interference cancellation IUS algorithms are considered for performance comparison: (i) successive multi-user detection (SMUD) [1] and (ii) successive ranging multi-user detection (SRMD) [2]. The simulations are performed in an Intel Core-i5 PC with 8 GB RAM.

A. Performance evaluation at low CFO

The value of CFO of every RT is uniformly distributed in $[-0.015, 0.015]$. Figure-1a shows the code detection performance by different algorithms. The code detection performance of all algorithms are

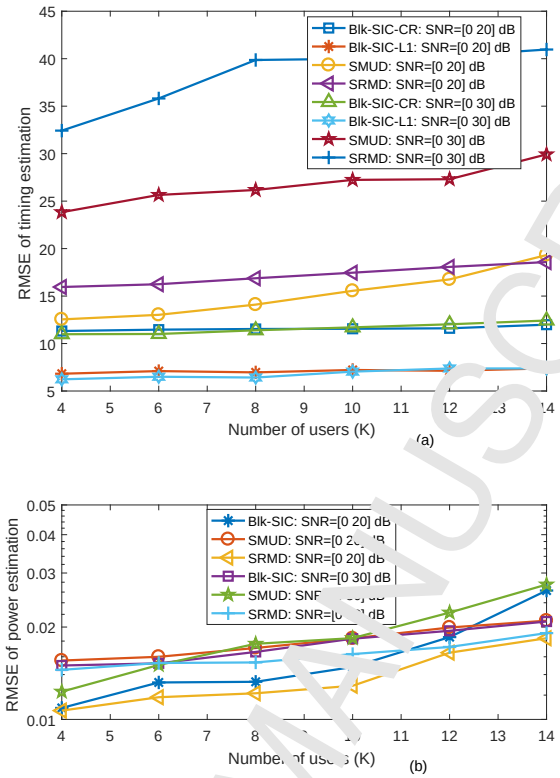

Fig. 2. IUS parameter estimation performances at low CFO. (a) RMSE of timing offset estimation. (b) RMSE of channel power estimation.

almost similar for low SNR variation i.e, $[0\ 20]$ dB. However, the performance of SMUD and SRMD drop quickly at relatively high SNR variation. In fact detecting users at large SNR variation is challenging. This is due to the fact that at larger SNR variation environment, the eNodeB receives very high signal energy from the RTs closer to the eNodeB whereas the received signal energy from far RTs are very small. The high SNR RTs act as interference sources to the low SNR RTs resulting in miss-detection of low power RTs. SMUD and SRMD generally try to detect every component of $\boldsymbol{h}_\ell$ separately whereas Blk-SIC tries to detect the whole energy of $\boldsymbol{h}_\ell$ by applying the block likelihood testing approach. Hence, BLk-SIC is less affected by the SNR variation. Figure-1b compares the computation time required by different algorithms. At $[0\ 30]$ dB environment with 4 RTs the computation time of Blk-SIC and SMUD are 0.0428 and 0.1325 sec respectively. Hence Blk-SIC is 3 times faster than SMUD. The time gap decreases with increasing the number of RTs. For example, with 12 RTs Blk-SIC is 2 times faster than SMUD. The computation time of SRMD is generally very high compared to other two algorithms.

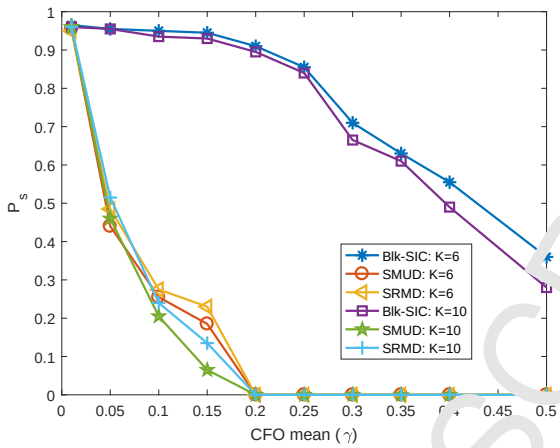

Fig. 3. Active code detection probability by different algorithms as a function of CFO mean. SNR variation [0 20] dB

Figure-2(a) shows the timing offset estimation performance by different algorithms. In general the proposed method outperforms SMUD and SRMD where SRMD performs the worst. As before, SMUD and SRMD are affected considerably by the SNR variation. At low SNR variations [0 20] and small number RTs, Blk-SIC-CR and SMUD performs similarly, however SMUD tends to degrading performance with increasing RTs. The RMSE of SMUD increases significantly for high SNR variation. In contrast, both Blk-SIC-CR and Blk-SIC-L1 remain almost unaffected with SNR variation whereas Blk-SIC-L1 performs the best. Figure-2(b) shows the channel power estimation error. The performance of all algorithms are almost similar where Blk-SIC exhibits moderate RMSE. Interestingly the performance of the algorithms are not much affected by the SNR variation.

B. Performance at large CFO

The value of CFO for every user is drawn from a normal distribution with mean $\mathfrak{h} \cdot \gamma$ and variance 10^{-4} where $\mathfrak{h}$ is the sign bit taking value from the set $\{+1, -1\}$ with equal probability. A larger value of γ denotes larger CFO for a RT. SNR variation is kept to [0 20] dB. Figure-3 compares the code detection performance of different algorithms as a function of CFO. At low CFO, SMUD and SRMD perform similarly to Blk-SIC. However, their performance degrade quickly with increasing CFO. For example, with $K = 6$ the P_s values of SMUD are $0.995, 0.44, 0.255$ and 0.185 for $\gamma = 0.01, 0.05, 0.1$ and 0.15 respectively. In contrast, the P_s value of Blk-SIC remains above 0.5 for $\gamma \leq 0.4$.

The CFO estimation accuracy by two different versions of Blk-SIC is illustrated in Figure-4(a). As can be seen the Blk-SIC-AD outperforms Blk-SIC-TLS. The performance gap of those algorithms are large at

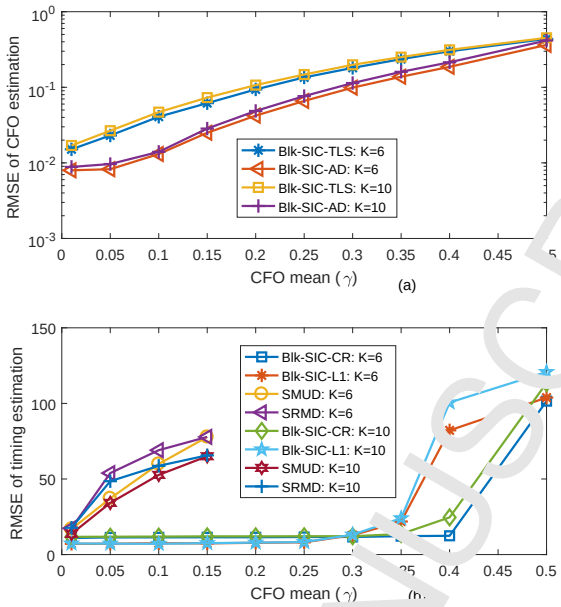

Fig. 4. (a) RMSE of CFO estimate. (b) RMSE of timing offset estimation as a function of CFO. SNR variation [0 20] dB

low CFO means, however they tends to close each other at higher CFO mean. As described in Section-IV-A, the complexity of Blk-SIC-AD is little higher than Blk-SIC-TLS. Hence, we achieve the good performance of Blk-SIC-AD forsake of little higher computational load. Finally, Figure-4(b) illustrates the effect of CFO on timing offset estimation accuracy. One important observation is that although Blk-SIC-L1 outperforms all other algorithms for moderate value of γ, i.e., $\gamma \leq 0.3$, its performance degrades for larger value of γ. The region behind the fact is that at larger value of γ the CFO estimation accuracy by Blk-SIC-AD degrades. As a result the estimation accuracy of $\bar{\boldsymbol{h}}_\ell$ is low. Consequently, the CIR estimate $\ddot{\boldsymbol{h}}_\ell$ by Blk-SIC-L1 in (29) generates many spurious peaks which results in inaccurate timing offset estimation. The situation can be improved by applying a hypothesis testing (see [11, Section-III-H] for a guideline).

VI. Conclusion

The dimension of IUS problem for future wireless networks is expected to increase significantly. In this work we provide a direction to reduce the problem dimension efficiently. Section-III shows that every block matrix of the IUS data model is ill-conditioned. Hence, CIR of every RT's can be represented compactly. We exploit the compact representation in Section-IV and develop the Blk-SIC algorithm that can work in presence of CFO. We also provide a direction for estimating noise variance which is

required for timing offset estimation. Finally, the advantage of using this data model is demonstrated using simulation results.

There are several interesting open questions that remains to be answered. The compact representation is made possible by some results from Fourier analysis. This might be interesting explore further in this direction in search of faster efficient algorithms. In addition, in [12] it was shown that the codebook itself impacts the detection-estimation performance significantly. Since the results presented herein makes way for larger codebooks, it is interesting to find systematic ways to design better codebooks. Finally, our approach to CFO estimation relies on a first order approximation in (7). It might be worthwhile to investigate we could avoid making such approximations.

APPENDIX

Recall that the $N \times N$ DFT matrix $\mathbf{F}$ is given by

$$[\mathbf{F}]_{k,j} = \exp\{-\mathrm{i}2\pi(k-1)(j-1)/N\}/\sqrt{N}.$$

and $\mathbf{\Theta}$ consists of m th through to $m+M-1$ th rows of the $M \times M$ identity matrix. The value of m is specified in the LTE standard. Then

$$\bar{\mathbf{F}} := \mathbf{\Theta}\mathbf{F} = \mathbf{F}_{(m:m+M-1\ ,\ 1:N_1)}.$$

We assume N large and $N \gg M$, which is also true in practice. To study the singular value distribution of $\bar{\mathbf{F}}$, consider $\mathbf{G} = \bar{\mathbf{F}}^*\bar{\mathbf{F}}$. The singular values of $\mathbf{F}$ are the square roots of the eigenvalues of $\mathbf{G}$. Now

$$\mathbf{G}_{k,\ell} = \frac{1}{N}\sum_{j=m}^{m+M-1} \exp\{\mathrm{i}2\pi(k-\ell)(j-1)/N\}.$$

Let us define $\bar{m} = m + (M-2)/2$.

$$\mathbf{G}_{k,\ell} = \frac{\exp\{\mathrm{i}2\pi(k-\ell)\bar{m}/N\}}{N} \times \sum_{j=m}^{m+M-1} \exp\{\mathrm{i}2\pi(k-\ell)(j-1-\bar{m})/N\}. \tag{32}$$

Next substitute $x = j - 1 - \bar{m}$. When $j = m$ then $x = m - 1 - \bar{m} = -1 - (M-2)/2 = -M/2$. When $j = m + M - 1$ then $x = M - 1 - (M-2)/2 = (2M - 2 - M + 2)/2 = M/2$. When $M \ll N$, we can very accurately approximate the sum in (32) as an integral:

$$\mathbf{G}_{k,\ell}\mathrm{e}^{-\mathrm{i}2\pi(k-\ell)\bar{m}/N} \approx \int_{-M/(2N)}^{M/(2N)} \exp\{\mathrm{i}2\pi(k-\ell)x\}\ \mathrm{d}x$$
$$= \frac{\sin\{\pi(k-\ell)M/N\}}{\pi(k-\ell)}. \tag{33}$$

Let us define

$$\mathbf{D} = \mathrm{diag}\{\ \mathrm{e}^{-\mathrm{i}2\pi\bar{m}.0},\ \ \mathrm{e}^{-\mathrm{i}2\pi\bar{m}.1},\ \ \cdots,\ \ \mathrm{e}^{-\mathrm{i}2\pi\bar{m}.(N_1-1)}\ \}$$

Then

$$\mathbf{G} \approx \mathbf{D}^*\mathbf{Q}\mathbf{D}$$

where

$$\mathbf{Q}_{k,\ell} = \frac{\sin\{\pi(k-\ell)M/N\}}{\pi(k-\ell)}$$

Since $\mathbf{D}$ is unitary, the eigenvalues of $\mathbf{G}$ and the eigenvalues of $\mathbf{Q}$ are almost identical. However, it is wellknown that about $(MN_1)/N$ eigenvalues of $\mathbf{Q}$ are very close to 1, and the rest are very close to 0 [33]. It should be noted that for practical values of N, M and N_1 the above approximation is highly accurate. For instance if we take $N = 24576, M = 839$ as per LTE specification, and $N_1 = 730$ associated with a cell radius 2.1 km, then the absolute relative difference between the eigenvalues of $\mathbf{G}$ and $\mathbf{Q}$ is below 4.6×10^{-5}.

REFERENCES

[1] M. Ruan, M. Reed, and Z. Shi, "Successive multiuser detection and interference cancelation for contention based OFDMA ranging channel," *Wireless Communications, IEEE Transactions on*, vol. 9, no. 2, pp. 481–487, 2010.

[2] C.-L. Lin and S.-L. Su, "A robust ranging detection with MAI cancellation for OFDMA systems," in *Advanced Communication Technology (ICACT), 2011 13th International Conference on*, 2011, pp. 937–941.

[3] L. Sanguinetti and M. Morelli, "An initial ranging scheme for the IEEE 802.16 OFDMA uplink," *Wireless Communications, IEEE Transactions on*, vol. 11, no. 9, pp. 3204–3215, 2012.

[4] D. H. Lee, "OFDMA uplink ranging for IEEE 802.16e using modified generalized chirp-like polyphase sequences," in *Internet, 2005.The First IEEE and IFIP International Conference in Central Asia on*, 2005.

[5] Y. Zhou, Z. Zhang, and X. Zhou, "OFDMA initial ranging for IEEE 802.16e based on time-domain and frequency-domain approaches," in *Communication Technology, 2006. ICCT '06. International Conference on*, 2006, pp. 1–5.

[6] X. Fu, Y. Li, and H. Minn, "A new ranging method for OFDMA systems," *Wireless Communications, IEEE Transactions on*, vol. 6, no. 2, pp. 659–669, 2007.

[7] S. Barbarossa, M. Pompili, and G. Giannakis, "Channel-independent synchronization of orthogonal frequency division multiple access systems," *Selected Areas in Communications, IEEE Journal on*, vol. 20, no. 2, pp. 474–486, 2002.

[8] Q. Wang, G. Ren, and J. W[illegible], "A centralized preamble detection-based random access scheme for lte comp transmission," *IEEE Transactions on Vehicular Technology*, vol. 65, no. 7, pp. 5200–5211, July 2016.

[9] V. N. X. Zhang, K. [illegible]aum and M. Cudak, "Ranging enhancement for 802.16e OFDMA PHY," *IEEE C802.16e-04/143*, 2004.

[10] Q. Wang and G. Ren, "Iterative maximum likelihood detection for initial ranging process in 802.16 OFDMA systems," *Wireless Communications, IEEE Transactions on*, vol. 14, no. 5, pp. 2778–2787, May 2015.

[11] M. M. Hyder and K. Mahata, "A sparse recovery method for initial uplink synchronization in OFDMA systems," *IEEE Transactions on Communications*, vol. 64, no. 1, pp. 377–386, Jan 2016.

[12] ——, "Zadoff-Chu sequence design for random access initial uplink synchronization in LTE-like systems," *IEEE Transactions on Wireless Communications*, vol. 16, no. 1, pp. 503–511, Jan 2017.

[13] ——, "Fast uplink synchronization in LTE-like systems," *IEEE Communications Letters*, vol. PP, no. 99, pp. 1–1, 2017.

[14] K. Wu, G. Ren, and Q. Wang, "Error vector magnitude analysis of uplink multiuser ofdma and sc-fdma systems in the presence of nonlinear distortion," *IEEE Communications Letters*, vol. 21, no. 1, pp. 172–175, Jan 2017.

[15] L. Sanguinetti, A. A. DAmico, M. Morelli, and M. Debbah, "Random access in massive mimo by exploiting timing offsets and excess antennas," *IEEE Transactions on Communications*, vol. 66, no. 12, pp. 6081–6095, Dec 2018.

[16] L. Sanguinetti, M. Morelli, and L. Marchetti, "A random access algorithm for LTE systems," *Transactions on Emerging Telecommunications Technologies*, vol. 24, no. 1, pp. 49–58, 2013.

[17] "3rd Generation Partnership Project; technical specification group radio access network; evolved universal terrestrial radio access (E-UTRA); physical channels and modulation (release 10)."

[18] Q. Wang, G. Ren, and J. Wu, "A multiuser detection algorithm for random access procedure with the presence of carrier frequency offsets in LTE systems," *IEEE Transactions on Communications*, vol. 63, no. 9, pp. 3299–3312, Sept 2015.

[19] Ericsson, "White paper: More than 50 billion connected devices," *Ericsson Tech Report*, vol. 284 23-3149 Uen, Feb 2011.

[20] J. Tropp, "Greed is good: algorithmic results for sparse approximation," *IEEE Transactions on Information Theory*, vol. 50, no. 10, pp. 2231 – 2242, Oct. 2004.

[21] S. Verdú, *Multiuser Detection*. Cambridge University Press, 1998. [Online]. Available: https://books.google.com.au/books?id=J-VuJDh3Ug8C

[22] Y. Eldar and M. Mishali, "Robust recovery of signals from a structured union of subspaces," *Information Theory, IEEE Transactions on*, vol. 55, no. 11, pp. 5302–5316, Nov 2009.

[23] H. L. Van Trees, *Detection, estimation, and modulation theory*, 1st ed. Wiley, Sep. 2001.

[24] J. Fuchs, "The generalized likelihood ratio test and the sparse representations approach," in *Image and Signal Processing*, ser. Lecture Notes in Computer Science, A. Elmoataz, O. Lezoray, F. Nouboud, D. Mammass, and J. Meunier, Eds. Springer Berlin Heidelberg, 2010, vol. 6134, pp. 245–253.

[25] A. Papoulis and U. Pillai, *Probability, Random Variables and Stochastic Processes*, 4th ed. McGraw-Hill Companies, Feb. 2002. [Online]. Available: http://www.amazon.com/exec/obidos/redirect?tag=citeulike07-20\&path=ASIN/0070484775

[26] J. A. Tropp, I. S. Dhillon, R. W. Heath, and T. Strohmer, "Designing structured tight frames via an alternating projection method," *IEEE Transactions on Information Theory*, vol. 51, no. 1, pp. 188–209, Jan 2005.

[27] H. Zhu, G. Leus, and G. B. Giannakis, "Sparsity-cognizant total least-squares for perturbed compressive sampling," *IEEE Transactions on Signal Processing*, vol. 59, no. 5, pp. 2002–2016, May 2011.

[28] P. Stoica, H. He, and J. Li, "New algorithms for designing unimodular sequences with good correlation properties," *IEEE Transactions on Signal Processing*, vol. 57, no. 4, pp. 1415–1425, April 2009.

[29] K. Mahata and T. Söderström, "Large sample properties of separable nonlinear least squares estimators," *IEEE Transactions on Signal Processing*, vol. 52, no. 6, pp. 1650–1658, June 2004.

[30] 3GPP-TS-36.101, "User equipment (UE) radio transmission and reception," *3rd Generation Partnership Project; Technical Specification Group Radio Access Network; Evolved Universal Terrestrial Radio Access (E-UTRA)*, 2012.

[31] D. Chu, "Polyphase codes with good periodic correlation properties (corresp.)," *Information Theory, IEEE Transactions on*, vol. 18, no. 4, pp. 531–532, Jul 1972.

[32] R. Frank and S. Zadoff, "Phase shift pulse codes with good periodic correlation properties (corresp.)," *Information Theory, IRE Transactions on*, vol. 8, no. 6, pp. 381–382, October 1962.

[33] D. Slepian, "Prolate spheroidal wave functions, Fourier analysis, and uncertainty - V: the discrete case," *The Bell System Technical Journal*, vol. 57, no. 5, pp. 1371–1430, May 1978.

CONFLICT OF INTEREST STATEMENT

Title of paper: Improved LTE like initial uplink synchronization via reduced problem dimension

Submitted to: Compute Communications

I, Md Mashud Hyder, author of the above mentioned paper certify that we have NO affiliations with or involvement in any organization or entity with any financial interest (such as honoraria; educational grants; participation in speakers' bureaus; membership, employment, consultancies, stock ownership, or other equity interest; and expert testimony or patent-licensing arrangements), or non-financial interest (such as personal or professional relationships, affiliations, knowledge or beliefs) in the subject matter or materials discussed in this manuscript.

Yours sincerely,

Md Mashud Hyder

Research Academic

School of Electrical Engineering and Computer Science

The University of Newcastle, Australia

Callaghan, NSW 2308, Australia.

Email : m.hyder@uon.edu.au